THE JOURNAL OF PHYSICAL CHEMISTRY LETTERS
A JOURNAL OF THE AMERICAN CHEMICAL SOCIETY

pubs.acs.org/JPCL

Letter

A Roadmap for Simulating Chemical Dynamics on a Parametrically Driven Bosonic Quantum Device

Delmar G. A. Cabral,[#] Pouya Khazaei,[#] Brandon C. Allen,[#] Pablo E. Videla,[#] Max Schäfer, Rodrigo G. Cortiñas, Alejandro Cros Carrillo de Albornoz, Jorge Chávez-Carlos, Lea F. Santos, Eitan Geva,[*] and Victor S. Batista[*]

Cite This: *J. Phys. Chem. Lett.* 2024, 15, 12042−12050

Read Online

ACCESS | Metrics & More | Article Recommendations | Supporting Information

ABSTRACT: Chemical reactions are commonly described by the reactive flux transferring the population from reactants to products across a double-well free energy barrier. Dynamics often involves barrier recrossing and quantum effects like tunneling, zero-point energy motion, and interference, which traditional rate theories, such as transition-state theory, do not consider. In this study, we investigate the feasibility of simulating reaction dynamics using a parametrically driven bosonic superconducting Kerr-cat device. This approach provides control over parameters defining the double-well free energy profile, as well as external factors like temperature and the coupling strength between the reaction coordinate and the thermal bath of nonreactive degrees of freedom. We demonstrate the effectiveness of this protocol by showing that the dynamics of proton-transfer reactions in prototypical benchmark model systems, such as hydrogen-bonded dimers of malonaldehyde and DNA base pairs, could be accurately simulated on the currently accessible Kerr-cat devices.

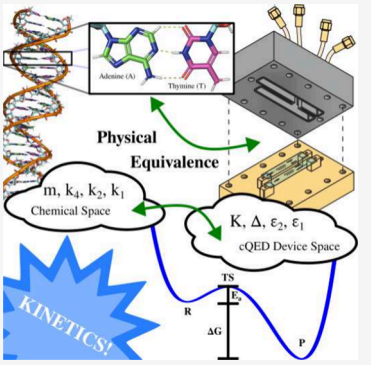

Computational modeling of reaction dynamics offers insights into the time scales and mechanisms of molecular transformations in chemical reactions, revealing the factors that determine the reaction rates and efficiencies. Most chemical reactions are multistep processes, with each step described by the reactive flux transferring across a barrier of a double-well potential energy surface along the reaction coordinate. However, simulating these elementary steps can be challenging, especially when barrier recrossing and significant quantum effects are involved, such as tunneling, zero-point energy, and interference. These factors lead to a complex interplay between coherence and dissipative dynamics, which are not accounted for by traditional rate theories such as transition-state theory.[1−6]

Recent advances in quantum engineering have generated interest in developing quantum devices to simulate the quantum dynamics of atoms, molecules, and condensed-phase systems.[7,8] Such analog quantum simulators can offer significant hardware efficiency advantage over general-purpose quantum computers, especially when the device Hamiltonian can be efficiently mapped onto the molecular system of interest. In this study, we explore the feasibility of using a Superconducting Nonlinear Asymmetric Inductive eLement (SNAIL) transmon[9] to simulate quantum dynamics of elementary chemical reactions. The SNAIL device develops a double-well structure when operated under a continuous drive with a frequency close to twice the SNAIL transmon resonance. This system is experimentally realizable in a superconducting quantum circuit and is referred to as Kerr-cat device.[10] Its controllable parameters can be adjusted to model the asymmetric double-well free energy profiles of various molecular systems across a wide range of external conditions, including temperature and coupling strength between the system and the thermal bath of nonreactive degrees of freedom. Here, we explore the capabilities of SNAIL devices by simulating the chemical dynamics of prototypical proton-transfer reactions in hydrogen-bonded complexes using the SNAIL Hamiltonian parametrized for malonaldehyde dimers and DNA base pairs, as could be experimentally implemented today on currently available platforms. These simulations are currently unattainable with noisy intermediate-scale quantum (NISQ) computers, including state-of-the-art conventional superconducting quantum computers, due to their circuit depth limitations. In contrast, we show that the SNAIL device could accurately capture the dynamics of these chemical reactions, effectively accounting for the delicate interplay among tunneling, zero-point energy, resonance, interference, and dissipative effects.

In transition-state theory (TST),[1−3] the reaction rate constant is given by the Eyring−Polanyi equation, $k_{TST} = \frac{k_B T}{h} e^{-\Delta G^{\ddagger}/k_B T}$. Here, $\Delta G^{\ddagger}$ is the Gibbs free energy of activation (the barrier height as measured from the minimum of the reactant well to the

Received: October 1, 2024
Revised: November 15, 2024
Accepted: November 20, 2024

https://doi.org/10.1021/acs.jpclett.4c02864
J. Phys. Chem. Lett. 2024, 15, 12042−12050

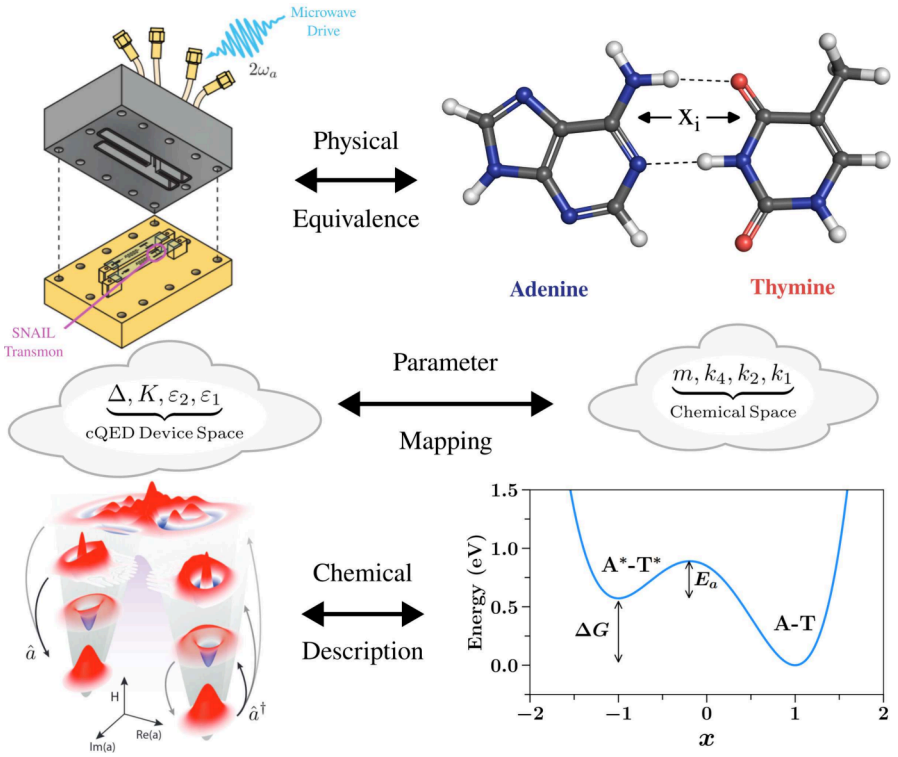

Figure 1. Schematic of the bosonic cQED device for quantum dynamics simulations in hydrogen-bonded complexes. Adapted from ref 25. Copyright 2024 American Chemical Society. The device is a half-aluminum, half-copper cavity resonator containing two sapphire chips with a SNAIL-transmon, readout resonator, and Purcell filter (top left).[36] A strong microwave drive at twice the resonance frequency converts the SNAIL-transmon Hamiltonian into the bistable Kerr-cat parametric oscillator Hamiltonian for analog simulations of quantum dynamics in molecular systems, such as the adenine-thymine dimer (top right). Parameters Δ, K, ϵ_1, ϵ_2 (middle left) are adjusted to map the effective Hamiltonian $\hat{H}_{KC}$ to the double-well Hamiltonian modeling the molecular system (middle right). The bottom left shows the Wigner transform phase space representation of the device quantum states, which are analogous to the states in the molecular double-well potential in the bottom right.

transition state configuration that corresponds to the barrier top), k_B is the Boltzmann constant, T is the absolute temperature, and h is the Planck constant. The Gibbs free energy of activation can be divided into enthalpy and entropy contributions: $\Delta G^{\ddagger} = \Delta H^{\ddagger} - T\,\Delta S^{\ddagger}$, where $\Delta H^{\ddagger}$ is the activation enthalpy and $\Delta S^{\ddagger}$ is the activation entropy. Identifying $\Delta H^{\ddagger}$ as the activation energy (E_a), the TST rate constant can be expressed by Arrhenius' law, $k_{TST} = A\, e^{-E_a/k_B T}$, with $A = \frac{k_B T}{h}\, e^{\Delta S^{\ddagger}/k_B}$ the rate constant for the barrierless case (i.e., when $\Delta H^{\ddagger} = E_a = 0$).

Deviations from TST and the Arrhenius law occur when the assumptions of these theories become invalid.[11,12] Recrossing events and quantum phenomena like tunneling, quantum interference, and zero-point energy effects can lead to deviations from TST by introducing reactive pathways beyond classical barrier crossing.[13] Some of those deviations can be approximately accounted for by the transmission coefficient κ, modifying the reaction rate constant to $k = \kappa k_{TST}$. This approach assumes that the reaction dynamics follows rate kinetics with a single well-defined rate constant. Another breakdown of TST occurs when the concept of a rate constant becomes invalid, such as when the barrier height is comparable to $k_B T$ or when the coupling between the reaction coordinate and other nonreactive molecular degrees of freedom (DOF) is weak.[14] These forms of TST breakdown often stem from the inherently quantum-mechanical nature of chemical dynamics.[15−17]

A prime example of an elementary chemical reaction of fundamental biological importance, which is often modeled using a double-well potential energy surface, is the adenine−thymine proton-transfer reaction in DNA.[18−20] The free energy profile for this reaction varies with the physiological conditions. Under normal cell conditions, the profile favors the hydrogen-bonded adenine−thymine complex form. However, during cell replication, this hydrogen bond must be broken to allow the DNA strands to duplicate. Proton transfer during this process has been suggested to cause spontaneous mutations due to bases occasionally adopting less likely tautomeric forms.[21] Therefore, simulating the dynamics of proton transfer in the adenine−thymine complex across a broad range of double-well free energy profiles can provide insights into the potential influence of quantum effects on the interconversion between tautomeric forms of the bases.

The traditional method for testing and validating chemical rate theories, including both TST/Arrhenius and post-TST/non-Arrhenius approaches, has relied on extensive experimental measurements of chemical dynamics across a diverse range of molecular systems and external conditions to cover both chemical space and parameters influencing chemical dynamics, such as temperature and the interactions between the reaction coordinate and the nonreactive DOF. However, this approach is highly challenging and labor-intensive. This is because experimentally monitoring reactant and product populations in real time may prove difficult, and changing from one chemical system to another often involves altering multiple parameters with complex and sometimes opposite effects. A notable example of the difficulty of this traditional approach is the 30-year delay between the theoretical prediction of the inverted

https://doi.org/10.1021/acs.jpclett.4c02864
J. Phys. Chem. Lett. 2024, 15, 12042−12050

region in the Marcus rate theory for electron-transfer reactions and its experimental validation.[22−24]

A promising alternative for experimentally testing and validating chemical rate theories has emerged with the advent of controllable and highly tunable quantum-mechanical platforms. These platforms can allow the exploration of quantum dynamics in various complex model systems across a broad range of parameter space.[7,8,25] Considering that chemical dynamics is inherently quantum mechanical in nature and that the most under-explored regimes of chemical dynamics exhibit significant quantum effects, these platforms can offer valuable simulation tools to investigate chemical reactivity under conditions that could be challenging for spectroscopic methods applied to molecular systems.[7]

Recent studies that exemplify this innovative approach of using quantum devices to explore chemical reactivity include the use of an ion trap platform as an analog simulator of the chemical dynamics underlying redox electron-transfer reactions.[26,27] Marcus theory, which describes the electron-transfer rate constant with a double-well model, is analogous to TST for nonredox chemical reactions. It employs a TST-like argument with an Arrhenius-type expression for the rate constant.[3] In Marcus theory, the transition state is the molecular configuration at the crossing point between the diabatic free energy profiles of the donor (reactant) and acceptor (product) states along the reaction coordinate associated with the reorganization of the nuclear DOF upon electron transfer. Like TST, Marcus theory treats the activation to the transition state as a classical process and assumes weak electronic coupling between the donor and acceptor states. Schlawin et al. demonstrated that an ion-trap device could reproduce the predictions of Marcus theory, including the inverted regime.[26] They also showed how this device could explore deviations from Marcus theory because of quantum (low-temperature) and strong electronic coupling effects. This enables the study of unconventional electron-transfer regimes that are challenging to capture using traditional methods.

In this Letter, we propose a novel strategy for simulating the dynamics of elementary reactions using a quantum platform. We explore the superconducting circuit quantum electrodynamics (cQED) Kerr-cat device.[25,28−34] We begin by introducing the device and highlighting the features that make it ideally suited for analog simulations of chemical dynamics. Next, we consider examples of molecular systems to demonstrate the Kerr-cat device capabilities as applied to simulating proton-transfer dynamics.

We begin by considering the effective Hamiltonian of the cQED Kerr-cat device, which constitutes an arrangement of a few Josephson junctions schematically shown in Figure 1:[28,35]

$$\hat{H}_{\mathrm{KC}} = \Delta\hat{a}^{\dagger}\hat{a} - K(\hat{a}^{\dagger})^2(\hat{a})^2 + \epsilon_2(\hat{a}^2 + \hat{a}^{\dagger 2}) + \epsilon_1(\hat{a} + \hat{a}^{\dagger}) \tag{1}$$

Here, $\hat{a}^{\dagger}$ and $\hat{a}$ are the ladder operators for the device bosonic mode, satisfying the usual bosonic commutator relation $[\hat{a}, \hat{a}^{\dagger}] = 1$. The Hamiltonian $\hat{H}_{\mathrm{KC}}$ includes adjustable parameters, namely the Kerr nonlinearity, K, the detuning parameter, Δ, and the drive coefficients, ϵ_1 and ϵ_2. These parameters can be experimentally altered by adjusting the magnetic flux and the amplitudes and frequencies of the microwave drives within the quantum device.[36]

Following Venkatraman et al.,[29] we assume that the noisy dynamics of the device can be described by the following Lindblad equation:

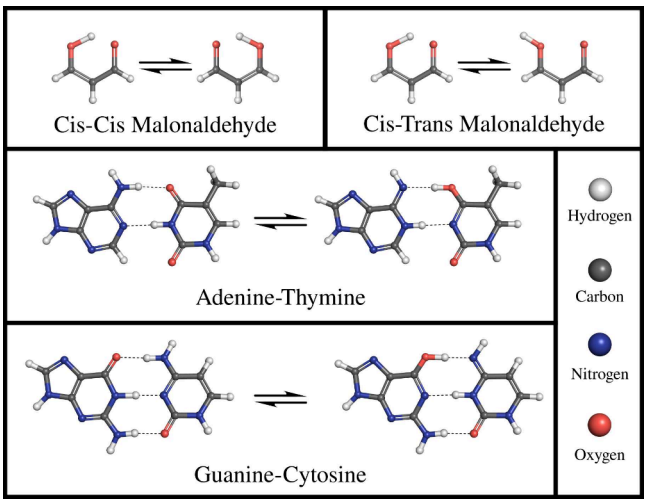

Figure 2. Hydrogen-bonded complexes studied to analyze intramolecular proton transfer in cis−cis and cis−trans malonaldehyde (top), intramolecular proton transfer in adenine−thymine (purine and pyrimidine) (middle), and guanine−cytosine (purine and pyrimidine) base pairs.

Table 1. Parameters Used to Simulate Double-Well Potentials for Proton Transfer in Molecular Systems, According to the Equation $V = k_4x^4 - k_2x^2 + k_1x$

System	k_4 [E_h/a_0^4]	k_2 [E_h/a_0^2]	k_1 [E_h/a_0]
Adenine−Thymine (DNA)[38]	1.4×10^{-3}	1.08×10^{-2}	5.2×10^{-3}
Guanine−Cytosine (DNA)[39]	7.7×10^{-4}	6.9×10^{-3}	4.5×10^{-3}
Malonaldehyde (cis−trans)[40,41]	9.4×10^{-5}	3.0×10^{-3}	2.9×10^{-3}
Malonaldehyde (cis−cis)[40,41]	7.1×10^{-4}	4.0×10^{-3}	0

$$\frac{\partial\hat{\rho}}{\partial t} = -\frac{i}{\hbar}[\hat{H}_{\mathrm{KC}}, \hat{\rho}] + \kappa(1 + n_{\mathrm{th}})\left(\hat{a}\hat{\rho}\hat{a}^{\dagger} - \frac{1}{2}\{\hat{a}^{\dagger}\hat{a}, \hat{\rho}\}\right) + \kappa n_{\mathrm{th}}\left(\hat{a}^{\dagger}\hat{\rho}\hat{a} - \frac{1}{2}\{\hat{a}\hat{a}^{\dagger}, \hat{\rho}\}\right) \tag{2}$$

where κ sets the photon loss rate corresponding to an effective dissipation rate due to coupling of the system with a surrounding environment and n_{th} represents the average thermal photon population, a quantity determined by the temperature. Like $\{K, \Delta, \epsilon_1, \epsilon_2\}$, the parameters κ and n_{th} are experimentally tunable and determine the noise associated with the experimental device.[37]

Consider also the model Hamiltonian for systems with a double-well potential energy surface given by

$$\hat{H}_{\mathrm{DW}} = \frac{\hat{p}^2}{2m} + k_4\hat{x}^4 - k_2\hat{x}^2 + k_1\hat{x} \tag{3}$$

which is commonly used to simulate hydrogen-bonded complexes.[18] The position and momentum operators of the reaction coordinate, $\hat{x}$ and $\hat{p}$, satisfy the commutation relation $[\hat{x}, \hat{p}] = i\hbar$. In the equation above, m represents the effective mass associated with motion along the reaction coordinate. The parameters $\{k_1, k_2, k_4\}$ are positive and real, typically determined by fitting the *ab initio* potential energy surface. This fitting process ensures the accurate representation of the barrier height, the curvature of the surface at the reactant and product wells, and the relative stability of reactants and products, as parametrized by k_1. Table 1 lists the parameters $\{k_1, k_2, k_4\}$ used in this study for numerical simulations of proton-transfer

https://doi.org/10.1021/acs.jpclett.4c02864
J. Phys. Chem. Lett. 2024, 15, 12042−12050

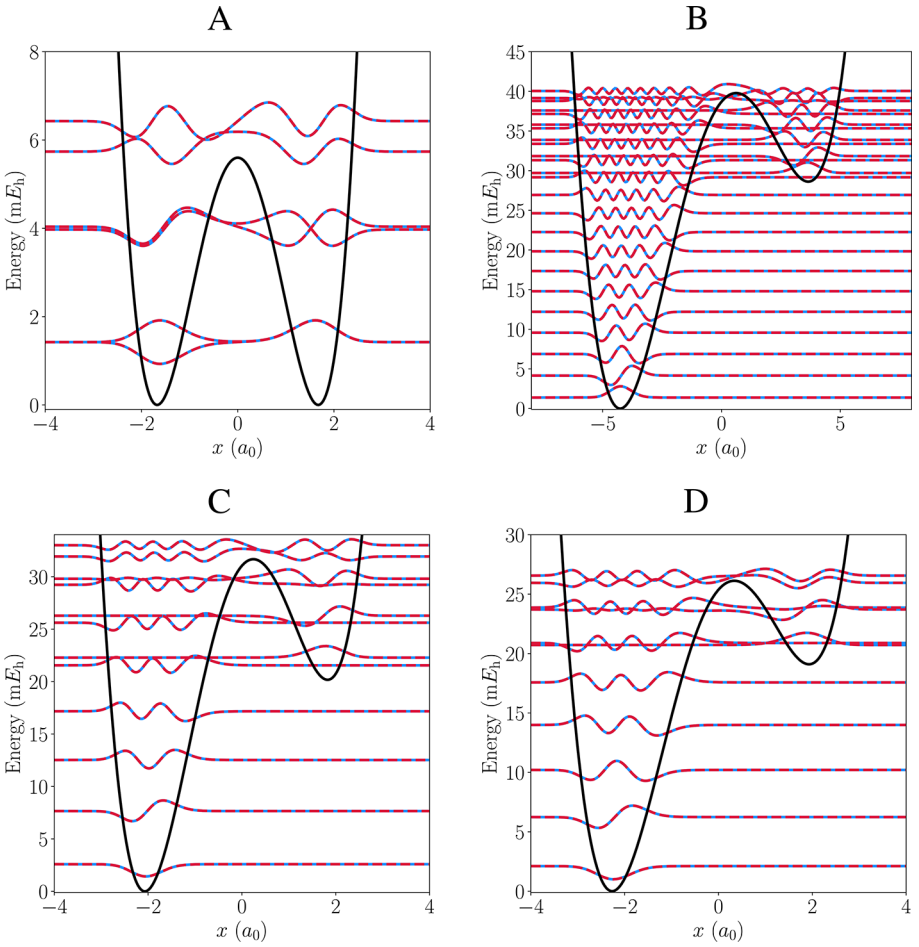

Figure 3. Eigenstates obtained by diagonalization of the model Hamiltonians for cis−cis malonaldehyde (A), cis−trans malonaldehyde (B), adenine−thymine (C), and guanine−cytosine (D), based on either the chemical double-well Hamiltonian (blue) or the Kerr-cat Hamiltonian (red) with $c = 0.1a_0$. Eigenstates are shown together with the potential energy surface as a function of the reaction coordinate "x".

dynamics (with m = 1836 amu) in the four model systems illustrated in Figure 2.

The next step is to map the Kerr-cat Hamiltonian, introduced in eq 1, onto the model Hamiltonian of the molecular system presented in eq 3. This requires mapping the photonic operators, $\{\hat{a}, \hat{a}^\dagger\}$, onto the reaction coordinate operators, $\{\hat{x}, \hat{p}\}$. To ensure the correct dynamics, this mapping must preserve the commutation relations: $[\hat{x}, \hat{p}] = i\hbar$ and $[\hat{a}, \hat{a}^\dagger] = \hat{1}$. A mapping that satisfies these conditions is given by

$$\hat{a} = \frac{1}{\sqrt{2}}\left(\frac{1}{c}\hat{x} + \frac{ic}{\hbar}\hat{p}\right), \quad \hat{a}^\dagger = \frac{1}{\sqrt{2}}\left(\frac{1}{c}\hat{x} - \frac{ic}{\hbar}\hat{p}\right) \tag{4}$$

where c is an arbitrary parameter with the same units as $\hat{x}$. Thus, the mapping of $\{\hat{a}, \hat{a}^\dagger\}$ onto $\{\hat{x}, \hat{p}\}$ is not unique. This flexibility in choosing c plays a crucial role in mapping the Kerr-cat Hamiltonian in eq 1 onto the chemical double-well Hamiltonian in eq 3. It should be noted that the value of c can be equivalent to the zero-point spread, $\sqrt{\hbar Z}$, if we define $\hat{x}$ and $\hat{p}$ as in ref 29.

Substituting the expressions for $\hat{a}$ and $\hat{a}^\dagger$ in terms of $\hat{x}$ and $\hat{p}$ from eq 4 into eq 1, we can recast the *negative* of the Kerr-cat Hamiltonian in terms of $\hat{x}$ and $\hat{p}$, omitting constant terms that do not impact the dynamics:

$$\begin{aligned} -\hat{H}_{\mathrm{KC}} = {} & \frac{c^2}{\hbar^2}(\epsilon_2 - K - \Delta/2)\hat{p}^2 + \frac{K}{4c^4}\hat{x}^4 \\ & - \frac{1}{c^2}(\epsilon_2 + K + \Delta/2)\hat{x}^2 - \frac{\epsilon_1\sqrt{2}}{c}\hat{x} + \frac{Kc^4}{4\hbar^4}\hat{p}^4 \\ & + \frac{K}{4\hbar^2}(\hat{x}^2\hat{p}^2 + \hat{p}^2\hat{x}^2) \end{aligned} \tag{5}$$

Comparing eq 5 with eq 3, we see that while $-\hat{H}_{\mathrm{KC}}$ includes $\hat{p}^2$, $\hat{x}^4$, $\hat{x}^2$, and $\hat{x}$ terms that can be mapped to the corresponding terms in the chemical double-well Hamiltonian (eq 3), it also contains additional terms ($\hat{p}^4$, $\hat{x}^2\hat{p}^2$, and $\hat{p}^2\hat{x}^2$) that are absent in eq 3.

We now map the parameters $\{\Delta, K, \epsilon_2, \epsilon_1\}$ onto $\{m, k_1, k_2, k_4\}$ by equating the coefficients of the $\hat{p}^2$, $\hat{x}^4$, $\hat{x}^2$, and $\hat{x}$ terms in eqs 3 and 5. This leads to the following mapping relations:

$$K = 4c^4k_4 \tag{6}$$

$$\epsilon_2 = \frac{\hbar^2}{4c^2m} + \frac{c^2k_2}{2} \tag{7}$$

$$\Delta = -\frac{\hbar^2}{2c^2m} + c^2k_2 - 8c^4k_4 \tag{8}$$

$$\epsilon_1 = -\frac{ck_1}{\sqrt{2}} \tag{9}$$

https://doi.org/10.1021/acs.jpclett.4c02864
J. Phys. Chem. Lett. 2024, 15, 12042−12050

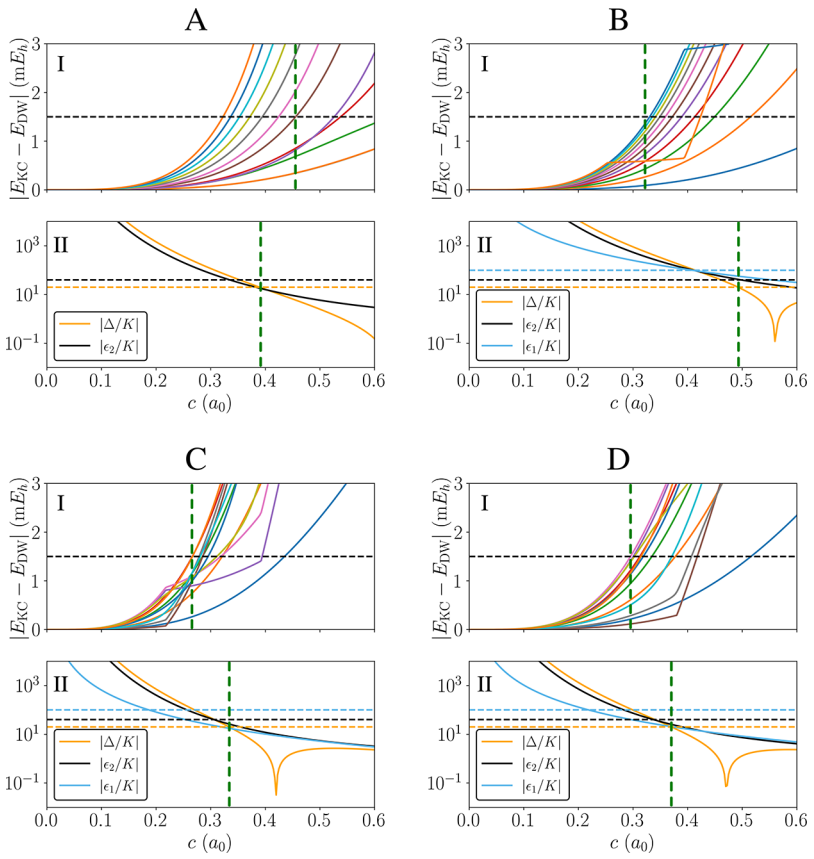

Figure 4. Absolute energy differences for the lower lying eigenstates of the chemical double-well and Kerr-cat Hamiltonian (panels I) and cQED device parameters (panels II) as a function of the scaling parameter c for cis−cis malonaldehyde (A), cis−trans malonaldehyde (B), adenine−thymine (C) and guanine−cytosine (D). The horizontal black dashed line in panel I indicates the threshold of chemical accuracy at 1.5 mE$_h$. The horizontal dashed lines in panels II indicate the maximum values of the parameters available in current cQED devices. The vertical dashed line indicates the maximum value of c recommended for accurate dynamics simulations (panels I) and minimum value of c ensuring experimental parameters available in existing cQED Kerr-cat platforms (panels II).[36]

Clearly, according to eqs 6−9, the values of $\{K, \Delta, \epsilon_2, \epsilon_1\}$ depend on the value of c. We then utilize the flexibility in choosing the value of c to minimize the effect of the additional terms $\hat{p}^4$, $\hat{x}^2\hat{p}^2$, and $\hat{x}^2\hat{p}^2$ in eq 3. As demonstrated in the Supporting Information (SI), this requires choosing a value of c small enough to satisfy the following inequality:

$$\frac{\hbar^2}{mk_2c^4} \gg 1 \tag{10}$$

Next, we compare the energy levels of the Kerr-cat and double-well Hamiltonians given by eq 5 and eq 3, respectively. In general, these energy levels are expected to be *different* due to the additional terms $\hat{p}^4$, $\hat{x}^2\hat{p}^2$, and $\hat{p}^2\hat{x}^2$ of the Kerr-cat Hamiltonian that are missing in the double-well Hamiltonian. However, the deviations between the energy levels of both Hamiltonians are expected to decrease as c becomes smaller [see eq 10 and Figure 4, which is explained below].

To establish an acceptable value of c, we set the tolerance for deviations between the energy levels of the Kerr-cat and double-well Hamiltonians at 1.5 mE$_h$ = 0.941 kcal mol^{-1}, which is a standard measure of chemical accuracy. It is crucial to note that accurate descriptions of barrier crossing dynamics require this level of accuracy not only for the ground state but also for energy levels up to the top of the barrier.

For example, the number of states required to capture accurate dynamics in the molecular model systems analyzed in this work is as follows: 6 for cis−cis malonaldehyde (Figure 3A), 24 for cis−trans malonaldehyde (Figure 3B), 12 for adenine-thymine (Figure 3C), and 14 for guanine-cytosine (Figure 3D). Ensuring that the energy levels of the Kerr-cat device, E_{KC}, and chemical double-well Hamiltonians, E_{DW}, are within chemical accuracy of each other ($E_{KC} - E_{DW}$ is below the horizontal dashed line in the panels I of Figure 4) also results in excellent agreement between their corresponding eigenfunctions, as shown in Figure 3.

Using the cQED device to encode $\hat{H}_{DW}$ requires a finite, nonzero value for the Kerr nonlinearity K, so the units of Δ, ϵ_2 and ϵ_1 are expressed in terms of K. For vanishingly small values of c, the ratios $\frac{\Delta}{K}$, $\frac{\epsilon_2}{K}$, and $\frac{\epsilon_1}{K}$ become very large (panels II of Figure 4), so they are experimentally unfeasible with current cQED platforms.[36] However, there exists a range of values of c for which the parameters are experimentally accessible while maintaining a useful degree of accuracy for the energies and stationary states. In particular, the Hamiltonian for the cis−cis malonaldehyde is experimentally accessible and meets the chemical accuracy criterion for stationary states and energies (Figure 4A). Chemical systems with asymmetric free energy profiles pose greater challenges due to the higher number of eigenstates required for addressing kinetic questions. Expanding the range of experimental parameters could enable an accurate simulation of these more challenging double-well problems,

https://doi.org/10.1021/acs.jpclett.4c02864
J. Phys. Chem. Lett. 2024, 15, 12042−12050

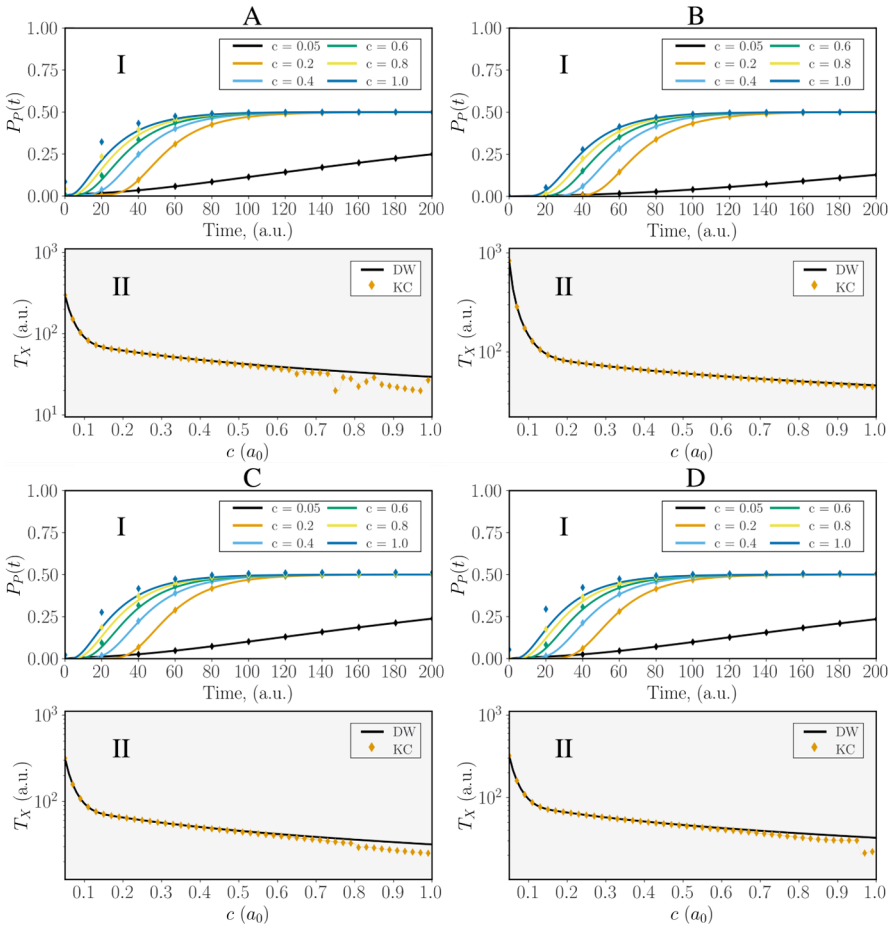

Figure 5. Comparison of observables obtained with $\hat{H}_{DW}$ (solid lines) and $\hat{H}_{KC}$ (diamonds) as a function of c, using $\kappa = 0.1$ and $n_{th} = 0.1$, for cis−cis malonaldehyde (A), cis−trans malonaldehyde (B), adenine−thymine (C) and guanine−cytosine (D). The time evolution of the product population is shown in the top subpanel (I), while the corresponding inverse reaction rate constants are shown in the bottom subpanels (II).

although it may also risk a breakdown of the effective Hamiltonian approximation.[36]

Consistency between the energy levels of the $\hat{H}_{KC}$ and $\hat{H}_{DW}$ Hamiltonians is necessary, but not sufficient to ensure that analog simulations on the Kerr-cat device accurately capture the chemical dynamics. This is because the *reaction rate* is also influenced by the coupling of the reaction coordinate to the thermal bath of *nonreactive* DOF. Consequently, the actual reaction rate constant depends not only on the eigenvalues and eigenfunctions of the Hamiltonian but also on the temperature and dissipation rate of the bath. Therefore, being able to simulate chemical dynamics on the Kerr-cat device requires that the dynamics of the device be dissipative (noisy), which is indeed the case. The noisy dynamics of Kerr-cat device are described by the Lindblad equation in eq 2 with an adjustable photon loss rate constant κ and temperature set by n_{th}.

In what follows, we consider a chemical system that experiences the same type of dissipation as the Kerr-cat device. This dissipative model is useful, as it results in chemical dynamics characterized by a reaction rate constant. However, other dissipation models could also be useful, as long as they capture the dissipation of the chemical system typically determined by the nature of its chemical environment and the way the reaction coordinate is coupled to the environment (e.g., the surroundings can correspond to liquid solution, biological environment, or solid-state environment). Hence, characterizing the dissipation of specific chemical systems and replicating it on a Kerr-cat device remain subjects of future studies that will focus on bath engineering.[42,43] It is noteworthy that Markovian and exotic dissipative channels can be engineered to a great extent in circuit QED.[44] The strength of dissipation in the squeezed Kerr oscillator experiment of Frattini and co-workers[28] is, for example, readily tunable by the amplitude of the microwave readout drive, and exotic forms of dissipation have been already demonstrated.[45,46]

Assuming that the chemical system undergoes the same type of dissipation as the Kerr-cat device, we use eq 4 to express the dissipator in eq 2 in terms of operators $\hat{x}$ and $\hat{p}$, which form the basis of the chemical double-well Hamiltonian in eq 3. This results in the following Lindblad equation for the chemical system:

$$\begin{aligned}\frac{\partial\hat{\rho}}{\partial t} &= -\frac{i}{\hbar}[\hat{H}_{DW}, \hat{\rho}] \\ &+ \frac{\kappa(1+2n_{th})}{4}\left[\frac{1}{c^2}([\hat{x}\hat{\rho}, \hat{x}] + [\hat{x}, \hat{\rho}\hat{x}])\right. \\ &\left. + \frac{c^2}{\hbar^2}([\hat{p}\hat{\rho}, \hat{p}] + [\hat{p}, \hat{\rho}\hat{p}])\right] \\ &- \frac{i\kappa}{4\hbar}([\hat{x}\hat{\rho}, \hat{p}] + [\hat{x}, \hat{\rho}\hat{p}] - [\hat{p}\hat{\rho}, \hat{x}] - [\hat{p}, \hat{\rho}\hat{x}])\end{aligned} \tag{11}$$

https://doi.org/10.1021/acs.jpclett.4c02864
J. Phys. Chem. Lett. 2024, 15, 12042−12050

The complete methodology for the numerical simulation of the open quantum dynamics is outlined in the SI. Here, we clarify that the initial state for dynamics propagation is localized in the reactant well, which is the higher-energy well in the above-mentioned chemical reactions. To generate this state, we diagonalize the system Hamiltonian and select the first eigenstate with more than 50% density in the reactant well. We then apply a sigmoidal filter function to remove the excess density outside of it (see SI for implementation details). This method creates a localized state and avoids the need to identify the critical points of each potential energy surface. By integrating eq 11 with an initial state $\hat{\rho}(0)$ localized in the reactant well, we obtain the time-evolved state $\hat{\rho}\ (t)$, which can be used to compute the product population at time t, as follows:

$$P_P(t) = \mathrm{Tr}\{\hat{\rho}(t)\hat{\Theta}_X\} \tag{12}$$

where $\hat{\Theta}_X$ is the Heaviside function:

$$\langle x|\hat{\Theta}_X|x'\rangle = \begin{cases} 0 & \text{for } x < 0 \\ \delta(x - x') & \text{for } x > 0 \end{cases} \tag{13}$$

The reactant-to-product reaction rate constant, $k = 1/T_X$, is obtained by fitting $P_P\ (t)$ to an exponential decay. The top subpanels of Figure 5 show the time evolution of $P_P\ (t)$ for the four proton-transfer reactions—cis malonaldehyde, cis−trans malonaldehyde, adenine−thymine, and guanine−cytosine—obtained by solving eq 11 for different values of c (solid lines). These top subpanels also include results where the chemical double-well Hamiltonian in eq 11, $\hat{H}_{DW}$, is replaced by the corresponding device Hamiltonian $-\hat{H}_{KC}$ with additional terms $\hat{p}^4$, $\hat{x}^2\hat{p}^2$, and $\hat{p}^2\hat{x}^2$ (diamonds). The bottom subpanels of Figure 5 show the dependence of the inverse reaction rate constant, T_X, on c for both $\hat{H}_{DW}$ (solid line) and $-\hat{H}_{KC}$ (diamonds).

A close examination of the results in Figure 5 reveals that the dynamics of both the chemical system and the Kerr-cat device align well, with the rate kinetics described by a rate constant. Additionally, the reaction rate constant shows significantly less sensitivity to the value of c compared to the energy levels and eigenfunctions of $\hat{H}_{DW}$ and $\hat{H}_{KC}$. Specifically, the rate constant predicted by the device matches that predicted for the chemical system at values of c as high as $0.4a_0$, much higher than the value of $c = 0.1a_0$ required to match energy levels and eigenfunctions near the top of the barrier. This is likely due to the effect of dissipation, making the overall dynamics less sensitive to small differences in the potential energy surface.

The results in Figure 5 were obtained with $\kappa = 0.1$ and $n_{th} = 0.1$, which are illustrative of the dissipation on the quantum device. However, the observed trends are insensitive to these specific values, as demonstrated by the rate constants obtained for various values of κ and n_{th} shown in Table 2 for $c = 0.1a_0$. As expected, T_X increases (i.e., the reaction slows down) when κ and n_{th} decrease. Nonetheless, the actual values of T_X for the chemical double-well and the Kerr-cat device are consistent, regardless of the κ and n_{th} values.

Conclusions. In this Letter, we proposed a novel approach to simulating chemical dynamics using a tunable Kerr-cat quantum device. This method allows for precise control over the parameters defining double-well potential energy surfaces as well as external factors such as temperature and dissipation rates. We demonstrated the efficacy of this approach by applying it to proton transfer in four prototypical hydrogen-bonded model complexes, showing that the underlying chemical dynamics can be accurately simulated on a quantum device.

Table 2. Inverse Reaction Rate Constants T_X (in $\hbar/E_h$) for Each Chemical System Obtained with the $\hat{H}_{DW}$ and $\hat{H}_{KC}$ Hamiltonians for Various κ and n_{th} Values with $c = 0.1a_0$

	Dissipation Constants (κ, n_{th})			
	(0.1, 0.1)	(0.1, 0.05)	(0.025, 0.1)	(0.025, 0.05)
Cis−cis Malonaldehyde (KC)	91 ± 1	91 ± 1	303 ± 4	295 ± 4
Cis−cis Malonaldehyde (DW)	91 ± 1	91 ± 1	303 ± 4	295 ± 4
Cis−trans Malonaldehyde (KC)	147 ± 2	142 ± 2	527 ± 7	499 ± 6
Cis−trans Malonaldehyde (DW)	147 ± 2	142 ± 2	528 ± 7	500 ± 6
Adenine−Thymine (KC)	95 ± 1	94 ± 1	323 ± 4	314 ± 4
Adenine−Thymine (DW)	95 ± 1	94 ± 1	323 ± 4	314 ± 4
Guanine−Cytosine (KC)	96 ± 1	95 ± 1	325 ± 4	316 ± 4
Guanine−Cytosine (DW)	96 ± 1	95 ± 1	325 ± 4	316 ± 4

Simulating chemical dynamics on a Kerr-cat device requires overcoming several challenges. A primary challenge addressed in this paper is mapping the chemical double-well Hamiltonian onto the Kerr-cat device Hamiltonian. This mapping is nontrivial, because the Kerr-cat device Hamiltonian includes additional terms ($\hat{p}^4$, $\hat{x}^2\hat{p}^2$, and $\hat{p}^2\hat{x}^2$), that are absent in the chemical Hamiltonian. We resolved this challenge by introducing a method that minimizes the impact of those additional terms by adjusting parameter c in the mapping of photonic operators $\hat{a}$ and $\hat{a}^\dagger$ to chemical operators $\hat{x}$ and $\hat{p}$. Specifically, we demonstrated that the energy levels and stationary states of the Kerr-cat and chemical Hamiltonians can be aligned (within chemical accuracy tolerance) by selecting a sufficiently small value of c. Furthermore, we found that reaction rate constants are even less sensitive to the value of c than the energy levels and stationary states, making them easier to reproduce when chemical dynamics are simulated on the Kerr-cat device.

The approach proposed in this Letter represents a significant first step toward enabling simulations of chemical dynamics on bosonic quantum simulators, which is beyond the capabilities of currently available NISQ computers. Remaining challenges include characterizing and engineering dissipation and designing devices that can reliably emulate more complex free energy surfaces beyond the one-dimensional asymmetric double-well free energy surfaces considered in this paper. Ongoing work addressing these challenges will be reported in future papers, paving the way for even more advanced simulations of quantum chemical dynamics on quantum devices.

■ ASSOCIATED CONTENT

Data Availability Statement

The Python code for the Hamiltonian analysis and dynamical simulations can be found at https://github.com/dcabral00/cQED4ChemDyn. The data files used to generate the figures in the manuscript are also provided at https://github.com/dcabral00/cQED4ChemDyn and hosted at 10.5281/zenodo.13694461.

Supporting Information

The Supporting Information is available free of charge at https://pubs.acs.org/doi/10.1021/acs.jpclett.4c02864.

Additional description of the Hamiltonian mapping, the simulation protocol, and benchmarks with experimental observations and dynamics figures for different dissipation parameters and computational basis sizes (PDF)

https://doi.org/10.1021/acs.jpclett.4c02864
J. Phys. Chem. Lett. 2024, 15, 12042−12050

Transparent Peer Review report available (PDF)

AUTHOR INFORMATION

Corresponding Authors

Eitan Geva − *Department of Chemistry, University of Michigan, Ann Arbor, Michigan 48109, United States;* orcid.org/0000-0002-7935-4586; Email: eitan@umich.edu

Victor S. Batista − *Department of Chemistry, Yale University, New Haven, Connecticut 06520, United States; Yale Quantum Institute, Yale University, New Haven, Connecticut 06511, United States;* orcid.org/0000-0002-3262-1237; Email: victor.batista@yale.edu

Authors

Delmar G. A. Cabral − *Department of Chemistry, Yale University, New Haven, Connecticut 06520, United States;* orcid.org/0009-0001-1195-5529

Pouya Khazaei − *Department of Chemistry, University of Michigan, Ann Arbor, Michigan 48109, United States*

Brandon C. Allen − *Department of Chemistry, Yale University, New Haven, Connecticut 06520, United States;* orcid.org/0000-0002-5512-1892

Pablo E. Videla − *Department of Chemistry, Yale University, New Haven, Connecticut 06520, United States;* orcid.org/0000-0003-0742-0342

Max Schäfer − *Department of Applied Physics and Physics, Yale University, New Haven, Connecticut 06520, United States; Yale Quantum Institute, Yale University, New Haven, Connecticut 06511, United States;* orcid.org/0009-0000-7871-014X

Rodrigo G. Cortiñas − *Department of Applied Physics and Physics, Yale University, New Haven, Connecticut 06520, United States; Yale Quantum Institute, Yale University, New Haven, Connecticut 06511, United States*

Alejandro Cros Carrillo de Albornoz − *Department of Applied Physics and Physics, Yale University, New Haven, Connecticut 06520, United States; Yale Quantum Institute, Yale University, New Haven, Connecticut 06511, United States; Department of Physics and Astronomy, University College London, London WC1E 6BT, U.K.*

Jorge Chávez-Carlos − *Department of Physics, University of Connecticut, Storrs, Connecticut 06511, United States*

Lea F. Santos − *Department of Physics, University of Connecticut, Storrs, Connecticut 06511, United States*

Complete contact information is available at: https://pubs.acs.org/10.1021/acs.jpclett.4c02864

Author Contributions

#D.G.A.C., P.K., B.C.A., and P.E.V. contributed equally to this work.

Notes

The authors declare no competing financial interest.

ACKNOWLEDGMENTS

The authors acknowledge support from the NSF Center for Quantum Dynamics on Modular Quantum Devices (CQD-MQD) under grant number 2124511. LFS and VSB acknowledge partial support from the National Science Foundation Engines Development Award: Advancing Quantum Technologies (CT) under Award Number 2302908. BCA, DGCA, and PEV acknowledge the Yale Center for Research Computing for allocation of computation time to perform the dynamics simulations on the Grace cluster. DGCA acknowledges Alexander Soudackov for helpful discussions regarding the adenine−thymine potential.

REFERENCES

(1) Eyring, H. The Activated Complex in Chemical Reactions. *J. Chem. Phys.* **1935**, *3*, 107−115.

(2) Truhlar, D. G.; Garrett, B. C.; Klippenstein, S. J. Current Status of Transition-State Theory. *J. Phys. Chem.* **1996**, *100*, 12771−12800.

(3) Nitzan, A. *Chemical dynamics in condensed phases: relaxation, transfer and reactions in condensed molecular systems*; Oxford University Press: New York, 2006.

(4) Pechukas, P. Transition State Theory. *Annu. Rev. Phys. Chem.* **1981**, *32*, 159−177.

(5) Laidler, K. J.; King, M. C. Development of transition-state theory. *J. Phys. Chem.* **1983**, *87*, 2657−2664.

(6) Pollak, E.; Talkner, P. Reaction rate theory: What it was, where is it today, and where is it going? *Chaos* **2005**, *15*, No. 026116.

(7) Altman, E.; Brown, K. R.; Carleo, G.; Carr, L. D.; Demler, E.; Chin, C.; DeMarco, B.; Economou, S. E.; Eriksson, M. A.; Fu, K.-M. C.; Greiner, M.; Hazzard, K. R.; Hulet, R. G.; Kollár, A. J.; Lev, B. L.; Lukin, M. D.; Ma, R.; Mi, X.; Misra, S.; Monroe, C.; Murch, K.; Nazario, Z.; Ni, K.-K.; Potter, A. C.; Roushan, P.; Saffman, M.; Schleier-Smith, M.; Siddiqi, I.; Simmonds, R.; Singh, M.; Spielman, I.; Temme, K.; Weiss, D. S.; Vučković, J.; Vuletić, V.; Ye, J.; Zwierlein, M. Quantum Simulators: Architectures and Opportunities. *PRX Quantum* **2021**, *2*, No. 017003.

(8) Georgescu, I. M.; Ashhab, S.; Nori, F. Quantum simulation. *Rev. Mod. Phys.* **2014**, *86*, 153−185.

(9) Frattini, N. E.; Vool, U.; Shankar, S.; Narla, A.; Sliwa, K. M.; Devoret, M. H. 3-wave mixing Josephson dipole element. *Appl. Phys. Lett.* **2017**, *110*, 222603.

(10) Frattini, N. E.; Cortiñas, R. G.; Venkatraman, J.; Xiao, X.; Su, Q.; Lei, C. U.; Chapman, B. J.; Joshi, V. R.; Girvin, S.; Schoelkopf, R. J. The squeezed Kerr oscillator: Spectral kissing and phase-flip robustness. *arXiv Preprint* **2022**, arXiv:2209.03934 DOI: 10.48550/arXiv.2209.03934.

(11) Yamamoto, T. Quantum Statistical Mechanical Theory of the Rate of Exchange Chemical Reactions in the Gas Phase. *J. Chem. Phys.* **1960**, *33*, 281−289.

(12) Chandler, D. Statistical mechanics of isomerization dynamics in liquids and the transition state approximation. *J. Chem. Phys.* **1978**, *68*, 2959−2970.

(13) Geva, E.; Shi, Q.; Voth, G. A. Quantum-mechanical reaction rate constants from centroid molecular dynamics simulations. *J. Chem. Phys.* **2001**, *115*, 9209−9222.

(14) Vazquez, F. X.; Talapatra, S.; Sension, R. J.; Geva, E. The Entropic Origin of Solvent Effects on the Single Bond *cZt-tZt* Isomerization Rate Constant of 1,3,5- *cis* -Hexatriene in Alkane and Alcohol Solvents: A Molecular Dynamics Study. *J. Phys. Chem. B* **2014**, *118*, 7869−7877.

(15) Miller, W. H. Quantum mechanical transition state theory and a new semiclassical model for reaction rate constants. *J. Chem. Phys.* **1974**, *61*, 1823−1834.

(16) Miller, W. H.; Schwartz, S. D.; Tromp, J. W. Quantum mechanical rate constants for bimolecular reactions. *J. Chem. Phys.* **1983**, *79*, 4889−4898.

(17) Miller, W. H. "Direct" and "Correct" Calculation of Canonical and Microcanonical Rate Constants for Chemical Reactions. *J. Phys. Chem. A* **1998**, *102*, 793−806.

(18) Godbeer, A.; Al-Khalili, J.; Stevenson, P. Modelling proton tunnelling in the adenine−thymine base pair. *Phys. Chem. Chem. Phys.* **2015**, *17*, 13034−13044.

(19) Soley, M. B.; Bergold, P.; Batista, V. S. Iterative power algorithm for global optimization with quantics tensor trains. *J. Chem. Theory Comput.* **2021**, *17*, 3280−3291.

(20) Soley, M. B.; Bergold, P.; Gorodetsky, A. A.; Batista, V. S. Functional tensor-train Chebyshev method for multidimensional

quantum dynamics simulations. *J. Chem. Theory Comput.* **2022**, *18*, 25−36.
(21) Watson, J. D.; Crick, F. H. Genetical implications of the structure of deoxyribonucleic acid. *Jama* **1993**, *269*, 1967−1969.
(22) Closs, G. L.; Miller, J. R. Intramolecular Long-Distance Electron Transfer in Organic Molecules. *Science* **1988**, *240*, 440−447.
(23) Miller, J. R.; Calcaterra, L. T.; Closs, G. L. Intramolecular long-distance electron transfer in radical anions. The effects of free energy and solvent on the reaction rates. *J. Am. Chem. Soc.* **1984**, *106*, 3047−3049.
(24) Marcus, R. A. Electron Transfer Reactions in Chemistry: Theory and Experiment (Nobel Lecture). *Angew. Chem., Int. Ed. Engl.* **1993**, *32*, 1111−1121.
(25) Dutta, R.; Cabral, D. G. A.; Lyu, N.; Vu, N. P.; Wang, Y.; Allen, B.; Dan, X.; Cortiñas, R. G.; Khazaei, P.; Schäfer, M.; Albornoz, A. C. C. d.; Smart, S. E.; Nie, S.; Devoret, M. H.; Mazziotti, D. A.; Narang, P.; Wang, C.; Whitfield, J. D.; Wilson, A. K.; Hendrickson, H. P.; Lidar, D. A.; Pérez-Bernal, F.; Santos, L. F.; Kais, S.; Geva, E.; Batista, V. S. Simulating Chemistry on Bosonic Quantum Devices. *J. Chem. Theory Comput.* **2024**, *20*, 6426−6441.
(26) Schlawin, F.; Gessner, M.; Buchleitner, A.; Schätz, T.; Skourtis, S. S. Continuously Parametrized Quantum Simulation of Molecular Electron-Transfer Reactions. *PRX Quantum* **2021**, *2*, No. 010314.
(27) So, V.; Suganthi, M. D.; Menon, A.; Zhu, M.; Zhuravel, R.; Pu, H.; Wolynes, P. G.; Onuchic, J. N.; Pagano, G. Trapped-Ion Quantum Simulation of Electron Transfer Models with Tunable Dissipation. *arXiv Preprint* **2024**, arXiv:2405.10368 DOI: 10.48550/arXiv.2405.10368.
(28) Frattini, N. E.; Cortiñas, R. G.; Venkatraman, J.; Xiao, X.; Su, Q.; Lei, C. U.; Chapman, B. J.; Joshi, V. R.; Girvin, S. M.; Schoelkopf, R. J.; Puri, S.; Devoret, M. H. Observation of Pairwise Level Degeneracies and the Quantum Regime of the Arrhenius Law in a Double-Well Parametric Oscillator. *Phys. Rev. X* **2024**, *14*, No. 031040.
(29) Venkatraman, J.; Cortinas, R. G.; Frattini, N. E.; Xiao, X.; Devoret, M. H. A driven quantum superconducting circuit with multiple tunable degeneracies. *arXiv Preprint* **2023**, arXiv:2211.04605 DOI: 10.48550/arXiv.2211.04605.
(30) Reynoso, M. A. P.; Nader, D. J.; Chávez-Carlos, J.; Ordaz-Mendoza, B. E.; Cortiñas, R. G.; Batista, V. S.; Lerma-Hernández, S.; Pérez-Bernal, F.; Santos, L. F. Quantum tunneling and level crossings in the squeeze-driven Kerr oscillator. *Phys. Rev. A* **2023**, *108*, No. 033709.
(31) Chávez-Carlos, J.; Lezama, T. L. M.; Cortiñas, R. G.; Venkatraman, J.; Devoret, M. H.; Batista, V. S.; Pérez-Bernal, F.; Santos, L. F. Spectral kissing and its dynamical consequences in the squeeze-driven Kerr oscillator. *npj Quantum Inf.* **2023**, *9*, 76.
(32) Iachello, F.; Cortiñas, R. G.; Pérez-Bernal, F.; Santos, L. F. Symmetries of the squeeze-driven Kerr oscillator. *J. Phys. A* **2023**, *56*, 495305.
(33) García-Mata, I.; Cortiñas, R. G.; Xiao, X.; Chávez-Carlos, J.; Batista, V. S.; Santos, L. F.; Wisniacki, D. A. Effective versus Floquet theory for the Kerr parametric oscillator. *Quantum* **2024**, *8*, 1298.
(34) Chávez-Carlos, J.; Reynoso, M. A. P.; García-Mata, I.; Batista, V. S.; Pérez-Bernal, F.; Wisniacki, D. A.; Santos, L. F. Driving superconducting qubits into chaos. *arXiv Preprint* **2024**, arXiv:2310.17698 DOI: 10.48550/arXiv.2310.17698.
(35) Frattini, N. Three-wave Mixing in Superconducting Circuits: Stabilizing Cats with SNAILs. Ph.D. Dissertation, Yale University, New Haven, CT, 2021. https://elischolar.library.yale.edu/gsas_dissertations/332.
(36) de Albornoz, A. C. C.; Cortiñas, R. G.; Schäfer, M.; Frattini, N. E.; Allen, B.; Cabral, D. G. A.; Videla, P. E.; Khazaei, P.; Geva, E.; Batista, V. S.; Devoret, M. H. Oscillatory dissipative tunneling in an asymmetric double-well potential. *arXiv Preprint* **2024**, arXiv:2409.13113 DOI: 10.48550/arXiv.2409.13113.
(37) Ding, A. Z.; Brock, B. L.; Eickbusch, A.; Koottandavida, A.; Frattini, N. E.; Cortinas, R. G.; Joshi, V. R.; de Graaf, S. J.; Chapman, B. J.; Ganjam, S.; Frunzio, L.; Schoelkopf, R. J.; Devoret, M. H. Quantum Control of an Oscillator with a Kerr-cat Qubit. *arXiv Preprint* **2024**, arXiv:2407.10940 DOI: 10.48550/arXiv.2407.10940.
(38) Godbeer, A. D.; Al-Khalili, J. S.; Stevenson, P. D. Modelling proton tunnelling in the adenine−thymine base pair. *Phys. Chem. Chem. Phys.* **2015**, *17*, 13034−13044.
(39) Slocombe, L.; Sacchi, M.; Al-Khalili, J. An open quantum systems approach to proton tunnelling in DNA. *Commun. Phys.* **2022**, *5*, 109.
(40) Ghosh, S.; Bhattacharyya, S. P. Dynamics of atom tunnelling in a symmetric double well coupled to an asymmetric double well: The case of malonaldehyde. *J. Chem. Sci.* **2012**, *124*, 13−19.
(41) Ghosh, S.; Talukder, S.; Sen, S.; Chaudhury, P. Optimised polychromatic field-mediated suppression of H-atom tunnelling in a coupled symmetric double well: two-dimensional malonaldehyde model. *Mol. Phys.* **2015**, *113*, 3826−3838.
(42) Murch, K.; Vool, U.; Zhou, D.; Weber, S.; Girvin, S.; Siddiqi, I. Cavity-assisted quantum bath engineering. *Phys. Rev. Lett.* **2012**, *109*, 183602.
(43) Kitzman, J.; Lane, J.; Undershute, C.; Harrington, P.; Beysengulov, N.; Mikolas, C.; Murch, K.; Pollanen, J. Phononic bath engineering of a superconducting qubit. *Nat. Commun.* **2023**, *14*, 3910.
(44) Shen, C.; Noh, K.; Albert, V. V.; Krastanov, S.; Devoret, M. H.; Schoelkopf, R. J.; Girvin, S. M.; Jiang, L. Quantum channel construction with circuit quantum electrodynamics. *Phys. Rev. B* **2017**, *95*, 134501.
(45) Sivak, V.; Eickbusch, A.; Royer, B.; Singh, S.; Tsioutsios, I.; Ganjam, S.; Miano, A.; Brock, B.; Ding, A.; Frunzio, L.; et al. Real-time quantum error correction beyond break-even. *Nature* **2023**, *616*, 50−55.
(46) Leghtas, Z.; Touzard, S.; Pop, I. M.; Kou, A.; Vlastakis, B.; Petrenko, A.; Sliwa, K. M.; Narla, A.; Shankar, S.; Hatridge, M. J.; et al. Confining the state of light to a quantum manifold by engineered two-photon loss. *Science* **2015**, *347*, 853−857.

https://doi.org/10.1021/acs.jpclett.4c02864
J. Phys. Chem. Lett. 2024, 15, 12042−12050